A NEW PULSE-MODULATION TECHNIQUE FOR GUIDANCE AND CONTROL OF AUTOMATED SPACECRAFT

Sam W. Thurman*
Jet Propulsion Laboratory, Pasadena, California
and
Henryk Flashner**
University of Southern California, Los Angeles, California

A comprehensive development of guidance laws applicable to such [asks as automated on-orbit rendezvous and soft landing on a planetary surface is presented for spacecraft employing pulse-opcra(cd (on-off) propulsion systems. The guidance problem is solved using a technique derived from robust control theory, leading to a new class of algorithms which modulate the duration and frequency of thruster firings. These algorithms do not depend upon dynamical approximations, and allow for analytical characterization of transient errors, limit cycle deadband region, and the set of possible terminal conditions in the design process. In addition, the desired performance is achievable in the presence of dynami cal mode] ing errors with known bounds; the effects of navigational errors can be minimized [o the extent that [hey can be bounded. This technique is also shown to be useful for attitude control. A realistic application is illustrated via computer simulation of a hypothe tical mission scenario, in which a robotic spacecraft equipped with an inertial guidance system performs a soft landing on the plane.[Mars,

* Graduate Student, Department of Aerospace Engineering, University of Southern California, University Park, Los Angeles, California 90089, and Member Technical Staff, Mars Pathfinder Project, Jet Propulsion Laboratory, 4800 Oak Grove Dr., Pasadena, Cal ifor nia 91109. Senior Member A[AA

** Associate Professor, Departments of Mechanical and Aerospace Engineering University of Southern California, University Park, Los Angeles, California 90069.

INTRODUCTION

Future exploratory missions have been proposed involving autonomous rendezvous and docking between two orbiting spacecraft and automatic landing on the surface of a planet, moon, or asteroid. Many of these missions will require simultaneous control of the trajectory and attitude of a space vehicle using a self-contaimd guidance, navigation], and control system. In previous missions, these functions have been performed in most cases through ground-based control or by piloted vehicles. There exists an extensive literature addressing spacecraft guidance techniques for automated orbital tram isfer, rendezvous, and soft landing. Much of (his knowledge base deals wi th the determination of trajectories and associated thrust profiles which minimize propellant consumpt ion; papers describing propulsive closed-loop guidance, techniques have focused on guidance laws for fixed or variable thrust propulsion systems which operate continuou sly. A representative, but not exhaustive, review of previous work is given below.

The theoretical aspects of rendezvous are discussed in the extensive survey paper by Jezewski *et al.*[1] Another survey paper, concentrating on rendezvous and docking operations issues, is (hat of Leonard and Bergmann.[2] Parten and Mayer,[3] and Young and Alexander[4] describe the rendezvous and docking procedures developed for t he *Gemin i* and *Apollo* piloted missions, respectively, which became the basis for the procedures used in Space Shuttle missions. 1 :xamples of automated rendezvous guidance schemes proposed for the Space Shut tle are the work of Olszewski[5] and Hanson and Deaton.[6] Some of the early work leading to the guidance algorithms used for lunar orbit insertion, landing, ascent, and on-orbit rendezvous i n the *Apollo* missions was performed by Cherry. [7] The *Apollo* lunar module guidance system is described by Klumpp.[8] Several guidance algorithms for continuously operated propulsion systems are given by Battin.[9] The automated guidance schemes used by the *Surveyor* and *Viking* spacecraft were similar; the terminal descent system developed for the *Surveyor* lunar lander is described by Cheng, Meredith, and Conrad,[10] while Ingoldby[11] has

documented the guidance techniques used for the *Viking* Mars landers. These vehicles employed sophisticated throttleable propulsion systems for powered descent and landing.

The design of on-board guidance systems is usually accomplished using linear approximations of the spacecraft's dynamics to obtain an analytically tractable problem. For autonomous operation, closed-loop guidance laws are sought; the optimization techniques surveyed by Jezewski *et al.*[1] generally yield open-loop thrust programs, which are highly susceptible to dynamical mismodeling. The performance of a conceptual system is often analyzed using extensive computer simulation to validate the approximations employed, a process which may be repeated several times as the design evolves and changes. Given the inherently nonlinear nature of pulse-operated thrusters, the closed-loop dynamics of a system employing these devices will be nonlinear even in cases where the spacecraft dynamics are otherwise linear. The use of pulsed thrusters for attitude control and station keeping presents similar problems. Control system design in these cases has been accomplished principally with phase-plane analysis techniques. For example, a pulse-frequency modulation technique for attitude control was developed by Farrenkopf, Sabroff, and Wheeler[12] using phase-plane methods and Lyapunov stability theory. The autopilot systems for the *Apollo* lunar module,[13] the *Viking* lander," and the Space Shuttle[14] have employed phase-plane type controllers. For guidance system design, the dynamical coupling between coordinate axes and between rotational and translational motion can make phase-plane analysis unwieldy and difficult.

This paper presents a new class of guidance and control laws for use with pulse-operated thrusters. These devices, which are relatively simple and low-cost, have been used extensively for attitude control and station keeping, but not for automated guidance in rendezvous and soft landing missions. The guidance problem is solved with an extension of robust nonlinear control theory, resulting in algorithms that determine the duration and frequency of thruster firings from estimates of spacecraft position and velocity. These algorithms utilize a complete nonlinear dynamical model

of the spacecraft motion, and allow for analytical characterization of transient error behavior, limit cycle deadband region, and the domain of possible terminal states. In addition, it is shown that the ric.sired performance is achievable in the presence of dynamical modeling errors with known bounds, and that the effects of navigation and attitude sensing errors can be minimized, given that appropriate bounds can be determined for these quantities. This approach is derived from robust control techniques, based on Lyapunov stability theory, that were pioneered by Corless and Leitmann.[15,16] Related techniques, such as sliding mode control, are described in the books by Utkin,[17] Slotine and Li,[18] and Vidyasagar.[19] Although the emphasis is on guidance, it is ultimately shown that the same technique is useful for attitude control and station keeping as well.

PROBLEM DESCRIPTION

A general form for the differential equations governing the motion of a space vehicle with mass $m(t)$ that is useful in rendezvous, soft landing, and station keeping applications is as follows:

$$m(t)\ddot{\mathbf{r}}(t) = m(t)\mathbf{g}[\mathbf{r}(t), \mathbf{r}_o(t)] + m(t)\mathbf{c}[\mathbf{r}(t), \dot{\mathbf{r}}(t), \mathbf{w}_F(t), \dot{\mathbf{w}}_F(t)] + \mathbf{f}_T(t) \qquad (1)$$

Equation (1) assumes a coordinate frame with its origin at some point O, that rotates with angular velocity $\mathbf{w}_F$ in inertial space. The three-dimensional vectors $\mathbf{r}$, $\dot{\mathbf{r}}$, and $\ddot{\mathbf{r}}$ denote the position, velocity, and acceleration of the spacecraft, respectively, in the rotating frame. The position of the origin, O, in an inertial frame is given by the vector $\mathbf{r}_o$. The vector functions $\mathbf{g}$ and $\mathbf{c}$ represent gravitational acceleration and Coriolis effects, respectively. The vector function $\mathbf{f}_T$ represents the applied thrust force. For orbital rendezvous problems, the point O is chosen to be the location of the target spacecraft; the rotating coordinate frame is aligned with t-o, taken to be the position of the target vehicle relative to the center of the attracting body, and rotates with $\mathbf{r}_o$. The same arrangement is also applicable to the station keeping problem: in this case $\mathbf{r}_o$ defines the desired orbit profile to be

maintained. In terminal descent problems, the vector $\mathbf{r}_o$ specifies the target landing silt, with the angular velocity of the rotating frame, $\mathbf{w}_F$, representing the rotation rate of the target body. An illustration of this type of coordinate frame for the terminal descent application is given in Fig. 1.

To perform a rendezvous, the relative position and velocity of the spacecraft must be simultaneously reduced to values small enough to permit successful docking with the target vehicle. A soft landing mission also requires simultaneous control of position and velocity, relative to a planetary surface, Station keeping, or orbit maintenance, is a logical extension of rendezvous, in which the station keeping spacecraft must essentially "rendezvous" with the desired orbit profile. repeatedly. These mission types are all conceptually similar in terms of the guidance objectives.

In many cases it is desired not only to control the terminal state vector of the spacecraft, but also to have it to follow a desired trajectory profile, in order to meet additional mission constraints. A more general version of Eq. (1) which accommodates this situation is given below. The six-dimensional spacecraft state vector is recast in terms of the guidance error vector, x, defined as

$$x(t) = \begin{bmatrix} \mathbf{r}(t) - \mathbf{r}_d(t) \\ \dot{\mathbf{r}}(t) - \dot{\mathbf{r}}_d(t) \end{bmatrix} \tag{2}$$

In Eq (2), $\mathbf{r}_d(t)$ and $\dot{\mathbf{r}}_d(t)$ represent the desired position and velocity profile of the spacecraft, respectively. Incorporating Eq. (2) into Eq. (1) yields the following differential equation for x:

$$\dot{\mathbf{x}} = Ax + \mathbf{B}[\mathbf{g}(\mathbf{r}, \mathbf{r}_o) + \mathbf{c}(\mathbf{r}, \dot{\mathbf{r}}, \mathbf{w}_F, \dot{\mathbf{w}}_F) - \ddot{\mathbf{r}}_d + \mathbf{a}_T] \tag{3}$$

where

$$A = \begin{bmatrix} \mathbf{0} & \mathbf{I} \\ \mathbf{0} & \mathbf{0} \end{bmatrix}, \quad \mathbf{B} = \begin{bmatrix} \mathbf{0} \\ \mathbf{I} \end{bmatrix} \tag{4}$$

In Eq. (3), the vector $\mathbf{a}_T$ is the thrust acceleration, which is equal to $\mathbf{f}_T(t)/m(t)$, and in Eq. (4), I is

the 3×3 identity matrix. For autonomous operation, a function of the form $\mathbf{f}_1 = \mathbf{f}(\mathbf{r}_d, \mathbf{x})$ specifying the commanded thrust vector is sought which will yield some desired closed-loop system.

PULSE-MODULATION GUIDANCE THEORY

For pulse-operated propulsion systems, guidance equations are needed which determine thrust vector magnitude and orientation commands, and provide the logic for their implementation. In this section a class of guidance equations applicable to two different thruster configurations is developed.

Analysis

The proposed class of functions for the commanded thrust vector, $\mathbf{f}_c$, consists of three components, as follows:

$$\mathbf{f}_c = \mathbf{f}_o(\mathbf{r}_d, \dot{\mathbf{r}}_d, \ddot{\mathbf{r}}_d, \mathbf{r}_o, \mathbf{w}_F, \dot{\mathbf{w}}_F, \mathbf{x}) + \mathbf{f}_f(\mathbf{x}) + \mathbf{f}_\varepsilon(\mathbf{x}) \tag{5}$$

The first component, $\mathbf{f}_o$, consists of feedback linearization terms which transform the original nonlinear system given by Eq. (3) into a nominally linear system:

$$\mathbf{f}_o = m\ddot{\mathbf{r}}_d - m[\mathbf{g}(\mathbf{r}_o, \mathbf{r}_d, \mathbf{x}) + \mathbf{c}(\mathbf{r}_d, \dot{\mathbf{r}}_d, \mathbf{w}_F, \dot{\mathbf{w}}_F, \mathbf{x})] \tag{6}$$

The second component, $\mathbf{f}_f$, is a linear feedback law designed to shape the closed-loop response of the transformed system using a constant gain matrix, designated $\mathbf{K}$:

$$\mathbf{f}_f = -m\mathbf{K}\mathbf{x} \tag{7}$$

The third component, $\mathbf{f}_\varepsilon$, is designed to simultaneously compensate for errors due to thrust mechanization with discrete thruster firings and other mismodeling of the spacecraft dynamics:

$$\mathbf{f}_\varepsilon = -mk(\mathbf{x}, t)\mathbf{n}[(1/\varepsilon)\mathbf{u}(\mathbf{x})] \tag{8}$$

The scalar function k and the vector functions n and u appearing in Eq. (8) are to be defined in the design process; the requirements they must satisfy are described in further detail below. In a more

general sense, a matrix function, $\mathbf{K}_\varepsilon$, can be used instead 01" k; here it is assumed for simplicity that KC = k], where 1 is the 3 x 3 identity matrix. The scalar parameter ε in Eq. (8) ultimately determines the accuracy with which the closed-loop system approximates the desired linear system, and will also be discussed subsequently.

In practice quantities such as the spacecraft position and velocity are not known precisely, but are estimated by an on-hoard navigation system or other sensors. Other parameters, such as the spacecraft mass, are not estimated but are known to fall within some bounded range. The commanded thrust components given in Eqs (6) through (8) are therefore computed as follows:

$$\mathbf{f}_c = \hat{m}\{\ddot{\mathbf{r}}_d - \hat{\mathbf{g}}(\hat{\mathbf{r}}_o, \mathbf{r}_d, \hat{\mathbf{x}}) - \hat{\mathbf{c}}(\mathbf{r}_d, \dot{\mathbf{r}}_d, \hat{\mathbf{w}}_I, \hat{\mathbf{x}}) - \mathbf{K}\hat{\mathbf{x}} - k(\hat{\mathbf{x}}, t)\mathbf{n}[(1/\varepsilon)\mathbf{u}(\hat{\mathbf{x}})]\} \tag{9}$$

In Eq. (9), x, $\mathbf{r}_o$, and m are denoted with hat symbols [o indicate the use of inexact estimates or nominal values for these parameters. The derivative of $\mathbf{w}_I$ is not shown in Eq. (9) because both it and $\mathbf{w}_F$ can be computed from r. in rendezvous and station keeping applications, and in soft landing applications $\mathbf{w}_F$ is very nearly constant for most target bodies of interest.

The actual thrust force at any instant will differ from the commanded value, with the extent of this difference depending primarily upon the number of discrete thrust levels available from the spacecraft's propulsion system. The applied thrust vector, $\mathbf{f}_T$, is

$$\mathbf{f}_T = \mathbf{C}\delta\mathbf{C}[\mathbf{C}^T\mathbf{f}_c + \delta\mathbf{f}_m^b] \tag{10}$$

In Eq. (10), the matrix $\mathbf{C}$ is the orthogonal transformation matrix between the spacecraft body-fixed reference frame mechanized in the spacecraft's computer, and the rotating frame used for the guidance computations. The matrix $\delta\mathbf{C}$ is the transformation matrix between the [rue space.craf(body frame and the computed body frame. The vector $\delta\mathbf{f}_m$ represents the applied thrust error due to quantization and any other types of thrust mechanization errors. The use of superscript b in Eq. (lo) denotes that the indicated vector is expressed in the body frame. If it is assumed that the attitude

determination errors embodied in the matrix $\delta \mathbf{C}$ are small (on the order of a few degrees), then $\delta \mathbf{C}$ can be accurately approximated as

$$\delta \mathbf{C} \approx \mathbf{I} + \delta \Theta \tag{11}$$

where

$$\delta \Theta = \begin{bmatrix} 0 & \delta\theta_z & -\delta\theta_y \\ -\delta\theta_z & 0 & \delta\theta_x \\ \delta\theta_y & -\delta\theta_x & 0 \end{bmatrix} \tag{12}$$

In Eq. *(12),* the parameters $\delta\theta_x$, $\delta\theta_y$, and $\delta\theta_z$ are small rotations about the *x*, y, and z computed body axes, respectively, which would bring the computed body frame into alignment with the true body frame. Using Eqs. (11) and (12), the applied thrust vector can be written as follows:

$$\mathbf{f}_T = \mathbf{f}_c + \delta \mathbf{f}_T \tag{13}$$

where

$$\delta \mathbf{f}_T \approx \mathbf{C} \delta \Theta \mathbf{C}^T \mathbf{f}_c + \mathbf{C}(\mathbf{I} + \delta \Theta) \delta \mathbf{f}_m^b \tag{14}$$

Iiu-(her characterization of $\delta \mathbf{f}_m$ requires spcci fic information about the number, thrust levels, and configuration of the thrusters comprising the propulsion system.

Using Eqs. (3), (4), (9), and (11) through (14), the closed-loop dynamical equations of the spacecraft can be written as follows:

$$\mathrm{x} = \mathrm{Ax} + \mathbf{B}\{\delta \mathbf{g} + \delta \mathbf{c} + (\delta \mathbf{f}_T / m) - (\delta m / m)\mathbf{f}_c - \mathbf{K}\hat{\mathbf{x}} - k(\hat{\mathbf{x}}, t)\mathbf{n}[(1/\varepsilon)\mathbf{u}(\hat{\mathbf{x}})]\} \tag{15}$$

In Eq. (1 5), the quantities $\delta \mathbf{g}$, $\delta \mathbf{c}$, and δm arc equal to $\mathbf{g} - \hat{\mathbf{g}}$, c - $\hat{\mathbf{c}}$, and $m - \hat{m}$, respectively. With further manipulation, Eq. (1 S) can be written as

$$\dot{\mathbf{x}} = [\mathrm{A} - \mathbf{B}\mathbf{K}]\mathbf{x} + \mathbf{B}\{\delta\mathbf{e} - k(\hat{\mathbf{x}}, t)\,\mathbf{n}[(1/\varepsilon)\mathbf{u}(\hat{\mathbf{x}})]\} \tag{16}$$

where

$$\delta\mathbf{e} = \delta\mathbf{g} + \delta\mathbf{c} + \mathbf{K}\delta\mathbf{x} + (\delta\mathbf{f}_T - \delta m\,\mathbf{f}_c)/m \tag{17}$$

In Eq. (17), the vector $\delta\mathbf{x}$ is equal to $\mathrm{x} - \hat{\mathbf{x}}$, and represents errors in the position and velocity estimates supplied by the spacecraft's navigation system.

The dynamical equations given by Eqs. (16) and (17) represent a nonlinear, nonautonomous system. The functions k, $\mathbf{n}$, and u and the parameter ε, comprising the $\mathbf{f}_\varepsilon$ component of the commanded thrust given in Eq. (8), ensure that the desired linear response is achieved. This is accomplished with a technique developed by Corless and Leitmann[15,16] for use with control actuators possessing a continuous and unbounded operating range, in which modeling uncertainties are treated in a deterministic, rather than a stochastic, manner. The key extension of their theory employed herein is the use of $\mathbf{f}_\varepsilon$ to compensate for *known* thrust mechanization errors caused by the use of pulse operated thrusters, as well as other, unknown modeling errors.

The properties required of k, n, and u are now stated. The function k is a positive, continuous, bounding function which must satisfy the following inequality:

$$k(\hat{\mathbf{x}}, t) \geq \|\delta\mathbf{e}\| \tag{18}$$

For the general case mentioned above, in which a matrix function $\mathbf{K}_\varepsilon$ is used instead of a scalar function k, Eq. (18) would be interpreted as requiring the norm of K_ε to be greater than the magnitude, or formally the Euclidean norm, of the vector $\delta\mathbf{e}$. The vector function n can be any continuous function with the following properties:

$$\begin{aligned} &(i) \quad \|\mathbf{u}\|\mathbf{n}(\varepsilon, \mathbf{u}) = \|\mathbf{n}(\varepsilon, \mathbf{u})\|\mathbf{u} \\ &(ii) \quad \|\mathbf{n}(\varepsilon, \mathbf{u})\| \geq 1 - \varepsilon/\|\mathbf{u}\|; \ \|\mathbf{u}\| > \varepsilon \end{aligned} \tag{19}$$

The vector function u is a linear function of the estimated guidance error vector, $\hat{\mathbf{x}}$, and another feedback matrix, designated I':

$$u = \mathbf{B}^T \mathbf{P} \hat{\mathbf{x}} \tag{20}$$

The matrix P is obtained from the *Lyapunov equation* given in Eq. (2 I) below. This equation has a unique solution that is symmetric and positive definite, provided that the matrix $\{A - \mathbf{BK} + \alpha \mathbf{I}\}$ has eigenvalues with only negative real parts, where a is a positive number suet] that α is greater than the real parts of the eigenvalues of [A - **BK**].[18,19] The matrix **Q** can be any positive definite matrix:

$$\mathbf{P}[\mathbf{A} - \mathbf{BK} + \alpha \mathbf{I}] + [\mathbf{A} - \mathbf{BK} + \alpha \mathbf{I}]^T \mathbf{P} + 2\mathbf{Q} = \mathrm{O} \tag{21}$$

The stability of the closed-loop system defined by Eqs. (16) through (2 I) will be evaluated using 1 .yapunov methods. [15-19] A *Lyapunov function candidate* is sought which indicates that in some region of the domain of **x** all trajectories **x**(*t*) arc *uniformly exponentially convergent* to within a small region of radius b *(i. e.,* $\|\mathbf{x}\| \leq b$) around the origin (x = O). Specifically, this system is exponentially convergent with rate α if for some positive constant β the following inequality is satisfied:[15]

$$\|\mathbf{x}(t)\| \leq b + \beta \|\mathbf{x}(t_o)\| \exp[-\alpha(t - t_o)]; \; t \geq t_o \tag{22}$$

The I.yapunov function candidate, designated *V(x),* to be used is $V(x) = \tfrac{1}{2}\mathbf{x}^T \mathbf{P} \mathbf{x}$, where the matrix 1' is obtained from Eq. (21). To validate Eq. (22), *V(x)* must possess the following properties:[20]

$$\begin{aligned} &(i) \qquad c_1 \|\mathbf{x}\|^2 \leq V(\mathbf{x}) \leq c_2 \|\mathbf{x}\|^2; \; c_1, c_2 > 0 \\ &(ii) \qquad \dot{V}(x) \leq -2\alpha [V(\mathbf{x}) - V^*]; \; V(X) > V^* \end{aligned} \tag{23}$$

Equation (23) represents a set of sufficient conditions only. The fact that a I.yapunov func(ion satisfying these conditions may not be found, or if for a given *V(x)* these conditions arc violate.{i for some value of **x**, does not by itself demonstrate that the origin of the closed-l(mp system is unstable. Condition (*i*) o! Eq. (23) is satisfied if *V(x)* is positive definite, which is the case since P is the

solution of Eq. (21). If condition *(ii)* is met, then Eq. (22) holds until a neighborhood around the origin with radius $b = (V^*/c_1)^{1/2}$ is reached. Once the state vector has entered the region $\|\mathbf{x}\| \le b$, it will remain there indefinitely. A detailed proof of these properties has been performed by Corless.[20]

To check condition *(ii) of* Eq. (23), the derivative of $V(x)$ is obtained using Eqs. (16) and (20):

$$\dot{V}(\mathbf{x}) = \mathbf{x}^T\mathbf{P}\dot{\mathbf{x}} = \mathrm{X}^T\mathbf{P}[\mathbf{A}-\mathbf{B}\mathbf{K}]\mathbf{x} + \mathbf{u}^T\{\delta\mathbf{e} - k(\hat{\mathbf{x}},t)\mathbf{n}[(1/\varepsilon)\hat{\mathbf{u}}]\} \tag{24}$$

In Eq. (24), the vectors u and $\hat{\mathbf{u}}$ are understood to represent $\mathbf{B}^T\mathbf{P}\mathbf{x}$ and $\mathbf{B}^{\prime}\mathbf{P}\hat{\mathbf{x}}$, respectively. To further develop this equation, the following expression is employed:

$$\mathbf{x}^T\mathbf{P}[\mathbf{A}-\mathbf{B}\mathbf{K}]\mathbf{x} = \tfrac{1}{2}\mathbf{x}^T\{\mathbf{P}[\mathbf{A}-\mathbf{B}\mathbf{K}] + [\mathbf{A}-\mathbf{B}\mathbf{K}]^T\mathbf{P}\}\mathbf{x} \tag{25}$$

Using condition *(i)* of Eq. (19), Eq. (21), and Eq. (25), further manipulation of Eq. (24) yields:

$$V(x) = -2\alpha V(\mathbf{x}) - \mathbf{x}^T\mathbf{Q}\mathbf{x} + \mathbf{u}\cdot\delta\mathbf{e} - k\|\mathbf{n}\|\mathbf{u}\cdot(\hat{\mathbf{u}}/\|\hat{\mathbf{u}}\|) \tag{26}$$

In Eq. (26), the arguments of the bounding function k have been dropped for simplicity. Noting that $\mathbf{u} = \hat{\mathbf{u}} + \delta\mathbf{u}$, where $\delta\mathbf{u} = \mathbf{B}^T\mathbf{P}\delta\mathbf{x}$, Eq. (26) becomes

$$\mathrm{v}(\mathrm{x}) = -2\alpha V(\mathbf{x}) - \mathbf{x}^T\mathbf{Q}\mathbf{x} + \|\hat{\mathbf{u}}\|[\delta\mathbf{e}\cdot(\hat{\mathbf{u}}/\|\hat{\mathbf{u}}\|) - k\|\mathbf{n}\|] + \delta\mathbf{u}\cdot[\delta\mathbf{e} - k\|\mathbf{n}\|(\hat{\mathbf{u}}/\|\hat{\mathbf{u}}\|)] \tag{27}$$

If the direction of $\delta\mathbf{u}$ relative to $\hat{\mathbf{u}}$ is assumed [o be arbitrary, then the following inequality can be constructed from Eq. (27):

$$\mathrm{v}(\mathrm{x}) \le -2\alpha V(\mathbf{x}) + 1: \tag{2 S')}$$

where

$$E \le \|\hat{\mathbf{u}}\|(\|\delta\mathbf{e}\| - k\|\mathbf{n}\|) + \|\delta\mathbf{u}\|(\|\delta\mathbf{e}\| + k\|\mathbf{n}\|) \tag{29}$$

Using the minimum requirements on k and $\|\mathbf{n}\|$ given in Eq. (18) and condition (ii) of Eq. (i 9), respectively, another inequality can be developed from Eqs. (27) and (29) that illustrates how k, n, and ε affect the region of convergence. The use. of these constraints yields

$$E \leq k\varepsilon(1+\|\delta\mathbf{u}\|/\|\hat{\mathbf{u}}\|) + \|\delta\mathbf{u}\|(\|\delta\mathbf{c}\|+k) \tag{30}$$

By establishing bounds on the terms in Eq. (30), an upper bound on E can be established. This, in turn, allows a suitable value of V^* to be determined using Eq. (23), and hence the radius 01 convergence, b, around the origin. The second term of Eq. (30) shows that navigational errors, which manifest themselves in $\delta\mathbf{u}$, impose a fundamental limitation on the smallest value of E that can be achieved in practice. In some situations this limitation may be less pronounced, depending upon the relative orientation of the $\delta\mathbf{u}$ and $\hat{\mathbf{u}}$ vectors over the course of the mission. Navigational data generated with a minimum variance estimation algorithm such as the Kalman filter have the property $\delta\mathbf{x}\cdot\hat{\mathbf{x}} = 0$ (SCC the book by Brown,[21] for example), which in (urn limits the magnitude of $\delta\mathbf{u}\cdot\hat{\mathbf{u}}$ in Eq. (27).

It should be noted that the theory presented above provides a sufficiently general framework for the synthesis of both explicit and implicit guidance laws. By making the vectors $\mathbf{r}_d$ and $\dot{\mathbf{r}}_d$ constant, with $\ddot{\mathbf{r}}_d = 0$, an explicit guidance law is obtained, in which the commanded thrust is a function only of the difference bet wccn the current esti mated spacecraft position and velocit y and the desired terminal state, specified by $\mathbf{r}_d$ and $\dot{\mathbf{r}}_d$. An implicit guidance law, in which the commanded thrust is derived from differences between the estimated flight path and a desired trajectory profile, is obtained when $\mathbf{r}_d$, $\dot{\mathbf{r}}_d$, and $\ddot{\mathbf{r}}_d$ arc chosen to be time-varying quantities.

Reaction Control System Configuration

A guidance law for usc with a reaction control system of small thrusters is illustrated below. This type of' system, used for attitude control, station keeping, and small (< 10--20 rids) maneuvers. provides a fixed thrust level in each of three orthogonal directions, in both a positive and negative sense, Some spacecraft, such as the Space Shuttle, carry enough thrusters to provide two or three different thrust levels along each axis. Equations (28), (29), and (30) will be used to characterize the behavior of stale trajectories in different regions of the domain of x. This presentation is a more

general version of a similar guidance law developed previously by the authors.[22]

Guidance Law. The relationship between the commanded and applied thrust for CaCh axis of a three-axis system is shown in Fig. 2. The hysteresis behavior that is characteristic of actual thrusters is also in Fig. 2, The $\mathbf{f}_o$ component of the commanded thrust vector is as given in Eq. (9). The f, component of the commanded thrust is a proportional-plus-derivative feedback law, as follows:

$$\mathrm{f}, = -m(K_P \Delta\hat{\mathbf{r}} + K_D \Delta\hat{\mathbf{v}}) \tag{31}$$

In Eq. (31), A? and $\Delta\hat{\mathbf{v}}$ comprise the estimate of the guidance error vector $\mathbf{x}$ *(i.e.,* $\hat{\mathbf{x}} = [\Delta\hat{\mathbf{r}}\ \Delta\hat{\mathbf{v}}\ ]^T$). From Fig. 2, the maximum error between the commanded and applied thrust prior to saturation is seen to be O. ST, where *T is* the thrust level of a single thruster. Assuming that thrust quantization errors arc dominant in Eq. (1 7), then $\|\delta\mathbf{e}\| \le T/2m$ (*m* in this case is the maximum spacecraft mass), and for the $\mathbf{f}_\varepsilon$ component of commanded thrust, the function *k* is also *T/2m*. The function n is

$$\begin{aligned} \mathbf{n}(\varepsilon, \hat{\mathbf{u}}) &= \mathbf{0}; & \|\hat{\mathbf{u}}\| &< \varepsilon \\ \mathbf{n}(\varepsilon, \hat{\mathbf{u}}) &= \hat{\mathbf{u}} / \|\hat{\mathbf{u}}\|; & \|\hat{\mathbf{u}}\| &\ge \varepsilon \end{aligned} \tag{32}$$

This form for n is chosen because it closely mimics the behavior of the thrusters. The vector $\hat{\mathbf{u}}$ is composed of the same feedback law used for f, in Eq. (31):

$$\hat{\mathbf{u}} = K_P \Delta\hat{\mathbf{r}} + K_D \Delta\hat{\mathbf{v}} \tag{33}$$

The Appendix describes a method for deriving feedback laws of this form from Eq. (21) by substituting $\mathbf{B}^T\mathbf{P}$ for the matrix K. In summary, the commanded thrust vector is

$$\mathbf{f}_c = m(\ddot{\mathbf{r}}_d - \hat{\mathbf{g}} - \hat{\mathbf{c}} - K_P \Delta\hat{\mathbf{r}} - K_D \Delta\hat{\mathbf{v}}) - (T/2)\,\mathbf{n}[(1/\varepsilon)(K_P \Delta\hat{\mathbf{r}} + K_D \Delta\hat{\mathbf{v}})] \tag{34}$$

Inaccessible Region. The existence of navigation errors will result in a region around the origin which cannot be reached with certainty. Equation (30) shows that *E* has a lower bound as follows: Using Eqs. (28) and (35), an expression defining this region can be obtained. An additional

$$E \leq \|\delta \mathbf{u}\|(T/m) \tag{35}$$

expression is needed (obtained from the Appendix), which bounds the Lyapunov function $V(x)$:

$$K_L\|\Delta\mathbf{r}\|^2 + K_D\|\Delta\mathbf{v}\|^2 - 2K_PK_D\|\Delta\mathbf{r}\|\|\Delta\mathbf{v}\| \leq V(\mathbf{x}) \leq K_L\|\Delta\mathbf{r}\|^2 + K_D\|\Delta\mathbf{v}\|^2 + 2K_PK_D\|\Delta\mathbf{r}\|\|\Delta\mathbf{v}\| \tag{36}$$

The parameter K_L in Eq. (36) appear-s in the matrix $\mathbf{P}$ used to obtain Eqs. (31) and (33), as shown in the Appendix. Combining Eqs. (28), (35), and (36) yields the desired expression:

$$K_L\|\Delta\mathbf{r}\|^2 + K_D\|\Delta\mathbf{v}\|^2 - 2K_PK_D\|\Delta\mathbf{r}\|\|\Delta\mathbf{v}\| \leq \|\delta\mathbf{u}\|T/(2\alpha m) \tag{37}$$

Deadband Region. The deadband in the thruster switching curve in Fig. 2 will result in exponential convergence to within a deadband region in the domain of $\mathbf{x}$ determined by the parameter ε in Eq. (32). Using Eqs. (30), (32) and (36), the following expression is obtained for this region:

$$K_L\|\Delta\mathbf{r}\|^2 + K_D\|\Delta\mathbf{v}\|^2 - 2K_PK_D\|\Delta\mathbf{r}\|\|\Delta\mathbf{v}\| \leq [\varepsilon + 3\|\delta\mathbf{u}\|]T/(4\alpha m) \tag{38}$$

Exponential Convergence Region. From Eq. (29), it is evident that the parameter E is no longer bounded when the magnitude of the commanded thrust vector exceeds the. capability of the propulsion system *(i.e.,* saturation). Beyond this point exponenti al convergence cannot be assured. Assuming that the effects of navigation errors arc relatively small, this region is defined by

$$m(\|\ddot{\mathbf{r}}_d\| + \|\mathbf{g}\| + \|\mathbf{c}\| + K_P\|\Delta\mathbf{r}\| + K_D\|\Delta\mathbf{v}\|) \leq T_{max} \tag{39}$$

In 1 'q. **(39),** T_{max} represents the maximum thrust capabi lit y of the propulsion syst cm. 1(should be noted that in some cases, especiall y rendezvous appl ications, the functions g and c from 1 :q. (1) can be strong functions of Ar and need to be represented as such in order to obtain a useful expression.

Asymptotic Convergence Region. The minimum requirement for assuring convergence of the state trajectories to within the dcadband region, regardless of rate, is [o have V(x)< O. Using Eqs. **(28),** (29), and (36) the following inequality is obtained describing this constraint:

$$(K_P^2 - \alpha K_L)\|\Delta \mathbf{r}\|^2 + K_D(K_D - \alpha)\|\Delta \mathbf{v}\|^2 + 2K_P K_D(1+\alpha)\|\Delta \mathbf{r}\|\|\Delta \mathbf{v}\| + (K_P\|\Delta \mathbf{r}\| + K_D\|\Delta \mathbf{v}\|)(\|\mathbf{a}_o\| - T_{max}/m) \le 0 \quad (40)$$

In Eq. (40), the term $\|\mathbf{a}_o\|$ is equal to $\|\mathbf{g}\| + \|\mathbf{c}\| + \|\ddot{\mathbf{r}}_d\|$. The potential dependence of the functions g and c, appearing in Eq. (1), on Ar must be taken into account in this case as well.

Clustered Engine Configuration

Spacecraft that must perform relatively large (> 100 rids) velocity changes may be equipped with multiple engines in a clustered arrangement, in order to provide an operating range of several discrete thrust levels. In this case the thrusters would likely be mounted parallel to one another. With this configuration, the thrust axis must be continually aligned by the attitude control system with the commanded thrust vector.

Guidance Law. The relationship between tbc commanded and applied thrust along the thrust axis is shown in Fig. 3, including the actual response of typical thrusters. The function **n in** this case is chosen 10 bc a variant of the saturation function:

$$\begin{aligned} \mathbf{n}(\varepsilon, \hat{\mathbf{u}}) &= \hat{\mathbf{u}}/\varepsilon; \qquad \|\hat{\mathbf{u}}\| < \varepsilon \\ \mathbf{n}(\varepsilon, \hat{\mathbf{u}}) &= \hat{\mathbf{u}}/\|\hat{\mathbf{u}}\|; \qquad \|\hat{\mathbf{u}}\| \ge \varepsilon \end{aligned} \quad (41)$$

This form of n avoids abrupt changes in the orientation of the commanded thrust vector, which could destabilize the operation of the spacecraft's attitude control system. As shown in Fig. 3, the maximum error between tbc commanded and applied thrust along the thrust axis, prior to saturation, is ().57', where 7' is again the thrust level of a single thruster. As the thrust level quantization error in each component of the guidance coordinate frame is a function of the commanded thrust vector orientation, a modified version of the *commanded* thrust expression of Eq. (34) is proposed for this case which is tailored to the characteristics of the thrust mechanization errors:

$$\mathbf{f}_c = \mathbf{f}_o + \mathbf{f}_f - \mathbf{K}_\varepsilon \mathbf{n}[(\quad/\varepsilon)(K_P\Delta\hat{\mathbf{r}} + K_D\Delta\hat{\mathbf{v}}) \tag{42}$$

where

$$\mathbf{f}_o + \mathbf{f}_f = m(\ddot{\mathbf{r}}_d - \hat{\mathbf{g}} - \hat{\mathbf{c}} - K_P\Delta\hat{\mathbf{r}} - K_D\Delta\hat{\mathbf{v}}) \tag{43}$$

and

$$\mathbf{K}_\varepsilon = \frac{T}{2}\begin{bmatrix} k_o + \sin|\theta| & 0 & 0 \\ 0 & k_o + \sin|\phi| & 0 \\ 0 & 0 & k_o + \cos\sqrt{\theta^2 + \phi^2} \end{bmatrix} \tag{44}$$

In Eq. *(42),* the function n is that of Eq. *(41).* The commanded thrust components in Eq. (43) arc unchanged from (heir counterparts in 1 :q. (34), The parameters θ and ϕ appearing in 1 :q. (44) arc the angles between the z axis of (hc guidance coordinate. frame and the projections of the vector sum $\mathbf{f}_o$ + f, in the *x*-z plane and the y-z p] ant, respectively. The parameter k_o must be greater than zero, and must be chosen to ensure that norm of the matrix KC satisfies Eq. (18); if k_o where equal to zero, this might not otherwise be the case when the angles θ and ϕ arc small.

Performance Analysis. With the guidance law proposed above, the inadmissible region, deadband region, exponential convergence region, and asymptotic con vergence region can be characterized by the same equations derived for the reaction control system. These are Eqs. (37), (38), (39), and (40), respectively. It should be noted that the use of these equations for the clustered engine configuration will generally lead to conservative results, since it is assumed that the thrust mechanization errors in each coordinate direction have [heir maximum possible value, regardless of the commanded thrust vector orientation. In terminal descent and landing applications, the thrust magnitude needed to compensate for the gravitational pull of the target body may result in at least one thruster firing continuously. The usc of the phrase "dcadband region" in this case is not meant in the literal sense.

MARS SOFT LANDING COMPUTER SIMULATION

in this section the guidance theory presented above is applied to the conceptual design of an integrated guidance, navigation, and control system for a hypothetical Martian soft lander. The performance of this vehicle is then investigated with a detailed digital computer simulation.

Mission and Spacecraft Description

The mission profile is illustrated in Fig. 1. The lander is transported to Mars in an entry vehicle that is carried by a cruise stage, which supports power generation, telecommunication, attitude determination and control, and midcourse propulsion functions during the interplanetary phase of the flight. The principal element of the lander's guidance system is an inertial navigation system, whose state vector is initialized 34 minutes prior to landing (L - 34 min in Fig. 1) with ground-based estimates of the spacecraft position and velocity vectors. The attitude matrix of the guidance system is established by an alignment process performed on-board the spacecraft. The alignment process is also used to calibrate the bias error components of the system's gyroscopes and accelerometers.

After initialization, the cruise stage's reaction control system is used to perform small maneuvers correcting any discrepancies between the flight path indicated by the guidance system and a stored trajectory profile, and for three-axis attitude control, Shortly before atmospheric entry, the entry vehicle is spun Up to 2 rpm by the cruise stage, which is then jettisoned. As the Martian surface approaches, a parachute is deployed to further slow the lander, and an on-board radar altimeter is activated. Once the radar system "locks on" to the surface, the lander separates from the entry vehicle backshell, actives its propulsion system, and completes its descent under automatic control. This mission profile is based on the entry and descent sequence for the *Mars Pathfinder* robotic spacecraft.[23] Unlike the guided lander simulated herein, *Mars Pathfinder* is an unguided vehicle which employs solid rocket motors for braking shortly before landing, yielding impact velocities of 101030 m/s; the vehicle cushions itself from the landing shock using an airbag system.

Kcy configuration data for the lander arc given in Table 1, The space.crafl's propulsion system is the clustered engine type of configuration described previously. This system consists of seven 445 N main thrusters and four 4.5 N thrusters for roll control. The thrusters employ hypergolic nitrogen tetroxide/hydraz ine propellants delivered by a blow-down pressurization system, and arc based on actual prototype hardware developed for small interceptor vehicles designed to destroy ballistic missiles.[24] By differential pulsing of engines offset from the nominal thrust axis, attitude control about the pitch and yaw axes is accomplished with the same thruster set used for guidance.

A high-level block diagram of the guidance, navigation, and control system is shown in Fig. 4. The spacecraft is equipped with a strapdown Inertial Measurement Unit (IMU) consisting of three ring-laser gyroscopes and three pendulous integrating acceler ometers, and a. smal 1 radar al timeter. The inertial instrument data arc. processed to mechanize the landing site-cent crcd rot sling coordinate frame of Fig. 1 in the spacecraft's flight computer, yielding indicated position, velocity, and attitude data (these quantities arc designated with a subscript i in Fig. 4), which along with a radar bias error parameter arc corrected by a sequential filter algorithm that processes altitude measurements from the radar system. The radar is a wide beamwidth (60 deg) firs[-return unit; that is, it measures the distance from the vehicle to the nearest point on the surface. The estimated position, velocity, and attitude parameters (indicated by a "hat" symbol in Fig. 4) arc used by the guidance law to compute the commanded thrust vector magnitude and orient ation, designated f_c and Θ_c in Fig. 4, respecti vc1 y. The commanded thrust vector orientation is then passed to the attitude control law for determination of the cornrnandcd moment vector, designated $\mathbf{m}_c$ in Fig. 4. The jet select logic in the engine controller issues firing commands to specific thrusters based on the values of $\mathbf{m}_c$ and f_c.

Using Eqs. (41) through (44), a guidance law for the lander was developed. The switching curve of Fig. 3 (for a cluster of seven engines instead of the five shown) was used by the engine controller. The elements of the matrix function KC appearing in 1 :q. (44) were chosen to compensate for thrust

mechanization errors due 10 the operation of the attitude control la w in addition to thrust level quantization errors in the switching curve of Fig. 3. An attitude control law with the same form as Eq. (34) was developed, with the appropriate terms from the rotational equations of motion substituted for the gravitational and Coriolis acceleration terms ((he functions g and c, respectively), and angular position and velocity feedback terms substituted for the translational position and velocity terms of Eq. (34). The guidance and attitude control law parameter values arc summarized in Table 2, The feedback gains given in Table 2 were obtained by solution of Eq. (48) in the Appendix, Commanded force and moment val ucs were computed and transmi ((cd to the engine controller every 20 ms (50 Hz rate), as indicated in Table 2. The engine controller issues commands to the thruster valves only when it detects a change in the requested state of a given thruster.

The error model for the inertial navigation system is summarized in Table 3. The instrumentation errors arc represented by mathematical models developed through extensive test and flight experience.[25] The performance of this system is representative of similar systems used in slmr(-range military aircraft and guided missiles. The initial position and velocity uncertainties represent the error covariance of the navigation system after propagation of the error covariance matrix at initialization, determined by liar[h-based radio tracking of the spacecraft, along the atmospheric entry trajectory to the point of radar lock-on (Britting[26] provides a detailed treatment of the error equations for inertial navigation systems). Navigational errors were. simulated by numerical integration of the error equations, using a pseudo-random number generator to sample the statistical distributions of the error sources described in Table 3. It is assumed that the inertial navigation equations are implemented in the flight computer with sufficient accuracy to make numerical computation errors negligible.

Simulation Proced u re

The dynamical behavior of the lander is simulated by numerical integration of equations representing the vehicle as a rigid body of variable mass with six degrees of freedom. Integration is

accomplished with a 7']' order variable step size Runge-Kutta method. The initial mass and moments of inertia arc determined using a pseudo-random number generator, according to a Gaussian distribution with statistics given in Table 1. Aerodynamic forces were not modeled due to (heir small effects in the thin Martian atmosphere. Center of mass modeling and calibration errors with respect to the thrust axis of the vehicle arc also simulated. Thrust level variations across successive thruster firings arc simulated by random number generation for each thruster, again according to the statistics Of Table 1. Due to the relatively slow variation of the navigation system errors, these quantities arc integrated with a 4^{th} order, fixed step size Runge-Kutta method. The time delay associated with the computations indicated in Fig. 4 is incorporated into the thruster dynamical model. The magnitude of this delay, found in Table 2, was estimated from an approximate count of the number of operations performed during each computation cycle. An average value of the time needed to pa-form the requisite operations on several modern flight computers was then determined.

At radar lock-on, the target landing site is designated 10 be the point directly beneath the lander. This results in the radar system viewing the same terrain during most of the descent, minimizing the effects of unknown terrain variations in the altitude data. If the commanded thrust vector has a positive z component (which can occur early in the descent), requiring the spacecraft to accelerate towards the surface, this component is ignored, and instead 0111 y the gravity compensation component is implemented, allowing the lander 10 continue at its current rate of descent. The guidance law uses constant values of $\mathbf{r}_d$ and $\dot{\mathbf{r}}_d$, chosen to target the spacecraft to a descent rate of 2 m/s at an altitude of lore. Once the spacecraft approaches these values to within the prescribed deadband region, the x and y target coordinates are reset to the current x and y position values indicated by the navigation system, in order to remove the effects of position errors from the commanded thrust vector, and a target altitude and descent rate of () m and I m/s, respectively, are commanded until touchdown occurs. This final segment is designed to minimize the horizontal velocity of the lander at touchdown.

Results

Results obtained from simulations representing three different scenarios are summarized below. The x and y components of initial position are zero in all cases. The lander is also assumed to be in a vertical orientation initially in each case. Case 1 represents an ideal scenario in which radar lock-on is achieved at a nominal 1500 m altitude and 70 m/s descent rate (see Fig. 1), with the lander having no initial downrange (x) or crossrange (y) velocity components. Case 2 represents a scenario in which radar lock-on occurs at an unexpectedly low altitude of 1100 m, and the lander has developed a 20 m/s downrange velocity on the parachute. Case 3 represents a "worst-case" scenario in which the lander achieves radar lock-on at the nominal altitude, but has developed unusually large downrange (40 rids) and crossrange (30 m/s) velocity components while on the parachute, and also has a relatively large descent rate of 80 m/s.

Contours defining the inaccessible, deadband, exponential convergence, and asymptotic convergence regions for the guidance law were developed using expressions based on Eqs. (37) through (40) and the data in Tables 2 and 3, and are shown in a two-dimensional space spanned by $\|\Delta \mathbf{r}\|$ and $\|\Delta \mathbf{v}\|$ in Fig. 5. Curves representing the actual trajectories obtained in the three simulation cases are also shown in Fig. 5. The velocity coordinate histories for Case 3, the worst-case scenario, are shown in Fig. 6. The depression angle relative to the $-z$ axis and the azimuth angle relative to the x axis of the commanded and actual thrust vectors for Case 3 are illustrated in Fig. 7. The commanded and actual thrust magnitude histories for Case 3 are shown in Fig. 8.

The lander required about 40 s to reach the surface in each scenario. The velocity component histories of Fig. 6 are representative of the response of a linear system, demonstrating that the pulse modulation guidance law does, in fact, yield the desired type of closed-loop behavior. In addition, Figs. 6 through 8 show that simultaneous control of the lander's translational and rotational motion can be successfully achieved with the same thruster set. The thrust vector orientation history of Fig.

7 shows that the guidance law initially commands a large pitch maneuver to null the downrange and crossrange velocity components quickly. Although radar contact with the surface is lost for thrust vector depression angles greater than 30 deg, the lander quickly recovers to a near-vertical orientation for the remainder of the descent, ensuring proper radar operation. The erratic behavior of the thrust vector azimuth angles in Fig. 7 occurs because this parameter becomes undefined as the depression angle approaches zero. Note that when the first target altitude of 10 m is reached and the lander redesignates the x and y position components of its target state, the guidance law briefly commands a roughly 15 deg pitch maneuver, The effect of this maneuver can also be seen in Fig. 6. This occurs because the guidance system is nulling small downrange and crossrange velocity components that developed earlier, duc to the buildup of x and y position errors in the inertial navigation system that could not be Sensed by the sequential filter from the altimeter data.

Note from Fig. 5 that in all three scenarios the initial conditions lie outside the asymptotic convergence region, and that the touchdown conditions are inside the "inadmissible" region, These characteristics serve 10 emphasize that predictions of performance derived from Lyapunov theory arc often exceeded in practice. In general, the simulation results of Figs. 5 through 8, along with additional simulation results not included herein, indicate that bounds on the behavior of guidance and control systems designed using Lyapunov-based techniques tend to be conservative.

ACKNOWLEDGEMENTS

The research described in this paper was carried out, in part, at the Jet Propulsion Laboratory (JPL), California Institute of Technology, under contract with the National Aeronautics and Space Administration. The authors extend their thanks to Mr. Stephen Bailey of JPL for developing the Mars lander spacecraft configuration, and to Mr. David Spencer, also of JPL for providing (hc *Mars Pathfinder* entry trajectory data used in the digital computer simulations.

APPENDIX

One useful technique for matching the feedback components of the commanded thrust, the vectors f, and $\mathbf{f}_c$ from Eqs. (7) and (8), respectively, is to set the gain matrix $\mathbf{K}$ in Eq. (7) equal to $\mathbf{B}^T\mathbf{P}$. As shown by Corless,[20] this yields the following *matrix Riccati equation*:

$$\mathbf{P}[\mathbf{A} + \alpha\mathbf{I}] + [\mathbf{A} + \alpha\mathbf{I}]^T\mathbf{P} - 2\mathbf{P}\mathbf{B}\mathbf{B}^T\mathbf{P} + 2\mathbf{Q} = 0 \tag{45}$$

The matrices $\mathbf{A}$ and $\mathbf{B}$ are given in Eq. (4). A class of solutions to Eq. (45) have the simple form:

$$\mathbf{P} = \begin{bmatrix} K_L\mathbf{I} & K_P\mathbf{I} \\ K_P\mathbf{I} & K_D\mathbf{I} \end{bmatrix} \tag{46}$$

The matrix $\mathbf{Q}$ used to obtain solutions conforming to Eq. (46) is as follows:

$$\mathbf{Q} = \begin{bmatrix} Q_P\mathbf{I} & \mathbf{0} \\ \mathbf{0} & Q_D\mathbf{I} \end{bmatrix} \tag{47}$$

Substitution of Eqs. (46) and (47) into Eq. (45) yields polynomial equations for K_D, K_P, and K_L:

$$\begin{aligned} &K_D^4 - 4\alpha K_D^3 + (5\alpha^2 - 2Q_D)K_D^2 + 2\alpha(2Q_D - \alpha^2)K_D + (Q_D^2 - 2\alpha^2 Q_D - Q),) = O \\ &K_P = \alpha(K_D - \alpha) + \sqrt{\alpha^2(K_D - \alpha)^2 + Q_P} \\ &K_L = 2K_P(K_D - a) \end{aligned} \tag{48}$$

Although multiple solutions to Eq. (48) exist, only one set of gains results in $\mathbf{P}$ being positive definite. For the correct solution, K_D, K_P, and K_L must be > 0, and $K_L K_D - K_P^2$ must *also* be > 0. As discussed earlier, the norm of the six-dimensional guidance error vector decreases exponentially with rate a. Within the exponential envelope established by a given a, the coefficients Q_P and Q_D appearing in Eq. (47) determine the amount 01 emphasis the resulting guidance law will place on nulling guidance errors in position relative to guidance errors in velocity.

REFERENCES

1. Jezewski, D. J., *et* al., "A Survey of Rendezvous Trajectory Planning," *Advances in the Astronautical Sciences,* Univelt, San Diego, Vol. 76, Part 11, 1992, pp. 1373-1396,

2. Leonard, C. 1,., and E. V. Bergmann, "A Survey of Rendezvous and Docking Issues and l)cvclopr~]cIIIs,'' Ac/\~[/rIce.Y *in the Astronautical Sciences,* Univelt, San Diego, Vol. 69, 19X9, pp. 85-101.

3. Parten, R. P., and J. P. Mayer, "Development of the Gemini Operational Rendezvous Plan," *Journal of Spacecraft and Rockets,* Vol. 5, No. 9, Sep. 1968, pp. 1023-1028.

4. Young, K. A., and J. D. Alexander, "Apollo Lunar Rendezvous," *Journal of Spacecraft and Rockets,* Vol. 7, No. 9, Sep. 1970, pp. 1083-1086.

5. Olszewski, O. W., "Automated Terminal Guidance for a Shuttle Rendezvous [o Space Station Freedom," *Proceedings of the AIAA Guidance, Navigation, and Control Conference*, Al AA, Washington, D.C., Vol. 1, 1990, pp. 377-387.

6. Hanson, J. M., and A, W. Deaton, "Guidance Schemes for Automated Terminal Rendezvous," AAS Paper 94-163, AAS/AIAA Spaceflight Mechanics Meeting, Cocoa Beach, Florida, Feb. 1994.

7. Cherry, G. W., "A Class of Unified Explicit Methods for Steering Throttleable and Fixed-Thrust Rockets," *Progress in Astronautics and Aeronautics,* Academic Press, New York, Vol. 13, 1964, pp. 689-726.

8. Klumpp, A. R., "Apollo Lunar Descent Guidance," *Automatica*, Vol. 10, 1974, pp. 133-146.

9. Battin, R. H., *An Introduction to the Mathematics and Methods of Astrodynamics*, Al **AA,** New York, **1987,** pp. **550-566,**

10 Cheng, R. K., Meredith, C. M., and D. A. Conrad, "Design Considerations for Surveyor Guidance," *Journal of Spacecraft and Rockets*, Vol. 3, No. 11, Nov. 1966, pp. 1569-1576.

11 Ingoldby, R. N., "Guidance and Control System Design of the Viking Planetary Lander," *Journal of Guidance and Control*, Vol. 1, No. 3, May-Jun. 1978, pp. 189-196.

12 Farrenkopf, R. 1.., Sabroff, A. E., and P. C. Wheeler, "Integral Pulse Frequency oil-on'" Control,"

Progress in Astronautics and Aeronautics, Academic Press, New York, Vol.13, 1964, pp. 185-230.

13. Widnall, W. S., "Lunar Module Digital Autopilot," *Journal of Spacecraft and Rockets*, Vol. *8,* No. 1, Jan. 1971, pp. *56-62.*

14. Bergmann, E. **V.,** Croopnick, S. R., Turkovich, J. J., and C. C. Work, "An Advanced Spacecraft Autopilot Concept," *Journal of Guidance and Control,* Vol. *2, No.* 3, May-Jun **1979,** pp. *161-168.*

15. Corless, **M.,** "Control of Uncertain Nonlinear Systems," *Journal of Dynamic Systems, Measurement, and Control,* Vol. 115, Jun. 1993, pp. 362-372.

16. Leitmann, G., "on One Approach to the Control of Uncertain Systems," *Journal of Dynamic Systems, Measurement, and Control*, **Vol. 115,** Jun. 1993, pp. 373-380.

17. Utkin, V. I., *Sliding Modes and Their Application to Variable Structure Systems,* MIR, Moscow, 1978.

18. Slotine, J. J., and W. Li, *Applied Nonlinear Control,* Prentice-Hall, Englewood Cliffs, 1991.

19. Vidyasagar, M., *Nonlinear Systems Analysis, 2nd* Ed., Prentice-Hall, Englewood Cliffs, **1993.**

20. Corless, M., "Guaranteed Rates of Exponential Convergence for Uncertain Systems," *Journal of optimization Theory and Applications*, Vol. 64, No. 3, Mar. 1990, pp. *481-494.*

21. Brown, R. G., *Introduction to Random Signal Analysis and Kalman Filtering*, Wiley, New York, 1983.

22, Thurman, S. W., and 11, Flashner, "Application of Nonlinear Control Techniques to Spacecraft Guidance for Rendezvous and Docking," AAS Paper 94-166, AAS/AIAA Spaceflight Mechanics Meeting, Cocoa Beach, Florida, Feb. 1994,

23. *Mars Pathfinder Mission Plan,* JPL Document D-11355 (internal document), Jet Propulsion Laboratory, Pasadena, California, December 1993,

24. Acampora, K. J., and H. Wichmann, "Component Development for Micropropulsion Systems," AIAA Paper 92-3255, AIAA/SAE/ASME/ASEE Joint Propulsion Conference, Nashville, Tennessee, Jul. 1992.

25. Savage, P. G., "Strapdown Sensors," *Strapdown Inertial Systems*, North Atlantic Treaty Organization AGARD Lecture Series No. 95, Technical Information Service, Springfield, Virginia, Jun. 1978.

26. Britting, K. R., *Inertial Navigation Systems Analysis,* Wiley, New York, **1971,** pp. **153-194.**

Table 1: Mars Lander Spacecraft Configuration Data

Parameter	*Nominal Value*	*RMS (1σ)* Variation
Initial Mass		
spacecraft (dry), kg	**220.0**	1.070
propellant/oxidizer, kg	**30.0**	**1.070**
Initial Moments of Inertia		
yaw (x-axis), kg-m'	**80.0**	2.0%
pitch (y-axis), kg-m'	**80.0**	**2.0%**
roll (z-axis), kg-m'	100.0	**2.00/0**
Center of Mass Offset, cm	0.0	**1.0**
Main Thrusters		
thrust level, N	**445.0**	**3.0%**
rise time, ms	**3.0**	·
max acceleration, m/s²	**12.5**	—
max pitch/yaw acceleration, rad/s²	1.11	—·
Roll Thrusters		
thrust level, N	4.45	3.0%
rise time, ms	1.0	—
max roll acceleration, rad/s²	0.10	—

Table 2: Guidance and Control System Parameters

Parameter	*Description*	*Value*
Computer Cycle Rate	frequency of command computations	50 Hz
Delay Time	computation time required for each command computer cycle	3 ms
Guidance Law		
α	guidance error rate of convergence	10 s^{-1}
Q_P	position weighting factor	,0-5 s^{-2}
Q_D	velocity weighting factor	,0.5
K_D	velocity feedback gain	0.2 s^{-1}
K_P	position feedback gain	0.02 s^{-1}
K_L	Lyapunov function parameter	0.004 s^{-3}
k_o	corrective acceleration scale factor	0.05
ε	guidance deadband parameter	0.02 m/s
Attitude Control Law		
α	attitude error rate of convergence	1 s^{-1}
Q_P	angular position weighting factor	,0.5 s^{-2}
Q_D	angular rate weighting factor	,0.5
K_D	angular rate feedback gain	4.0 s^{-1}
K_P	angular position feedback gain	8.0 s^{-2}
K_L	Lyapunov function parameter	48 s^{-3}
k	corrective acceleration (pitch/yaw)	1.11 s^{-1}
k_r	corrective acceleration (roll)	0.10 s^{-2}
&	attitude deadband parameter	0.07 s^{-2}

Table 3: Inertial Navigation System Error Model

Parameter	RMS (1σ) *Value*	*Units*
Landing Site Elevation Error	**300**	m
Initial Position Error	**5.18 (altitude)** **7.55 (downrange)** **1.04** (crossrange)	km
Initial Velocity Error	**6.36 (altitude)** **1.13 (downrange)** **1.96** (crossrange)	m/s
Initial Attitude Error	**0.33 (each axis)**	deg
IMU Misalignment	18	arcsec
Gyro Error Model		
bias calibration error	**0,10**	deg/hr
time-varying bias [a]	**0.05**	deg/hr
scale factor error	**100**	ppm
time-varying scale factor [a]	**25**	ppm
scale factor asymmetry	**10**	ppm
time-varying asymmetry [a]	**10**	ppm
random walk	0.10	deg/hr$^{1/2}$
Accelerometer Error Model		
bias calibration error	**50**	μg
scale factor error	**100**	ppm
scale factor asymmetry	**25**	ppm
compliance (g^2)	1.0	μg/g^2
white noise	**1.0**	mm/s
Radar Altimeter Error Model		
proportional bias [b]	0.003	n/a
white noise	**0.20**	m

modeled as first-order Gauss-Markov processes with time constants of 1 hr

' modeled as first-order Gauss-Markov process with time constant of 3 min

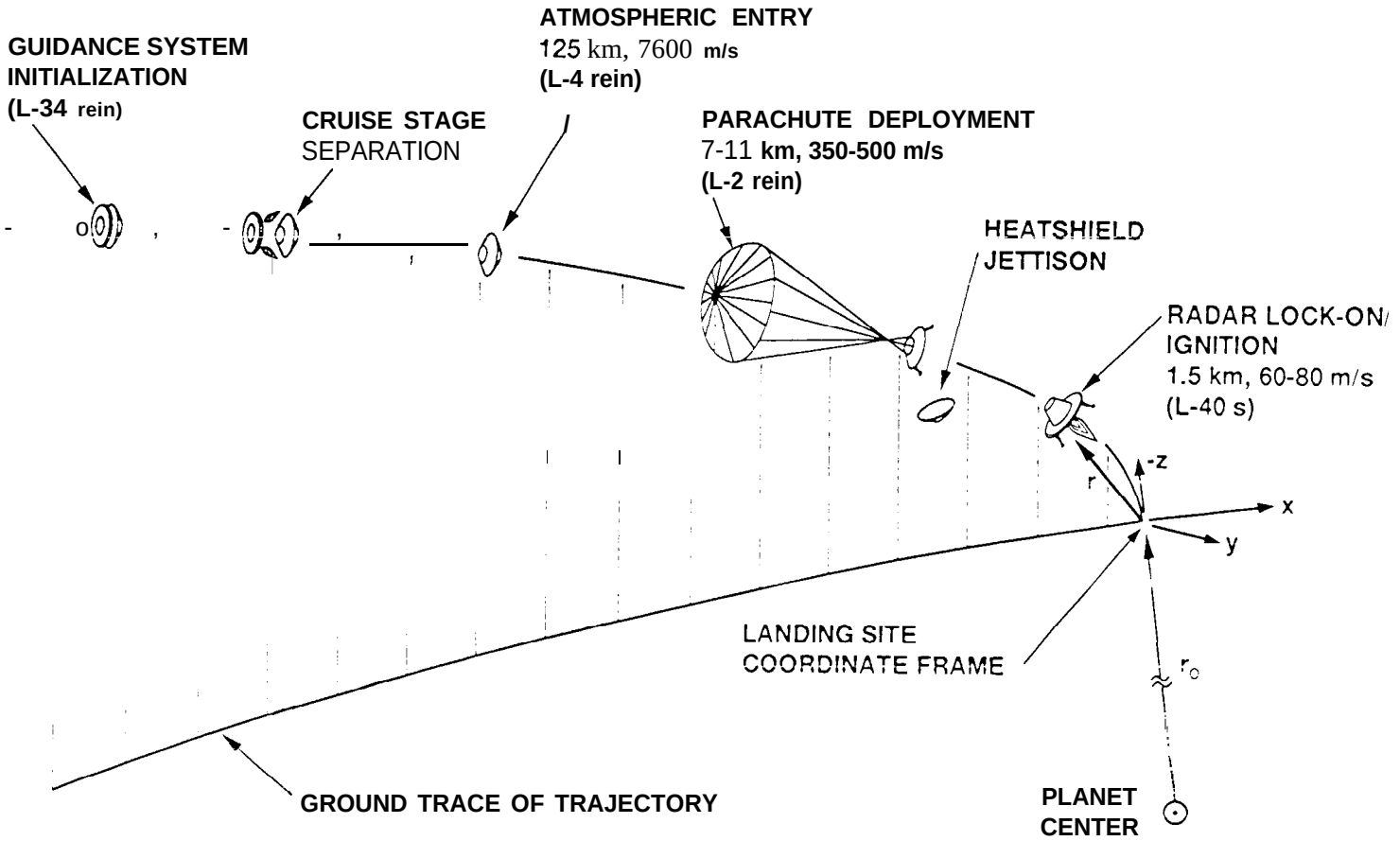

Figure 1: **Mars Lander Mission Profile**

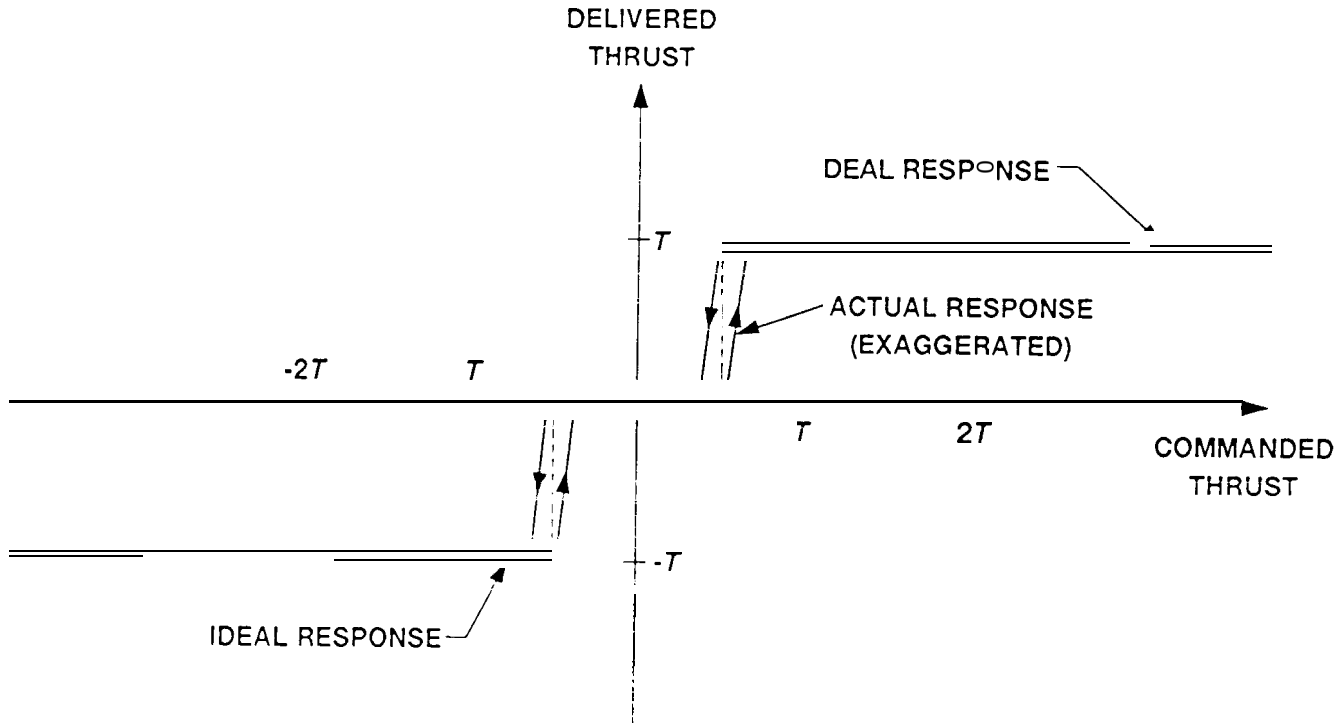

Figure 2: Switching Curve for Reaction Control System

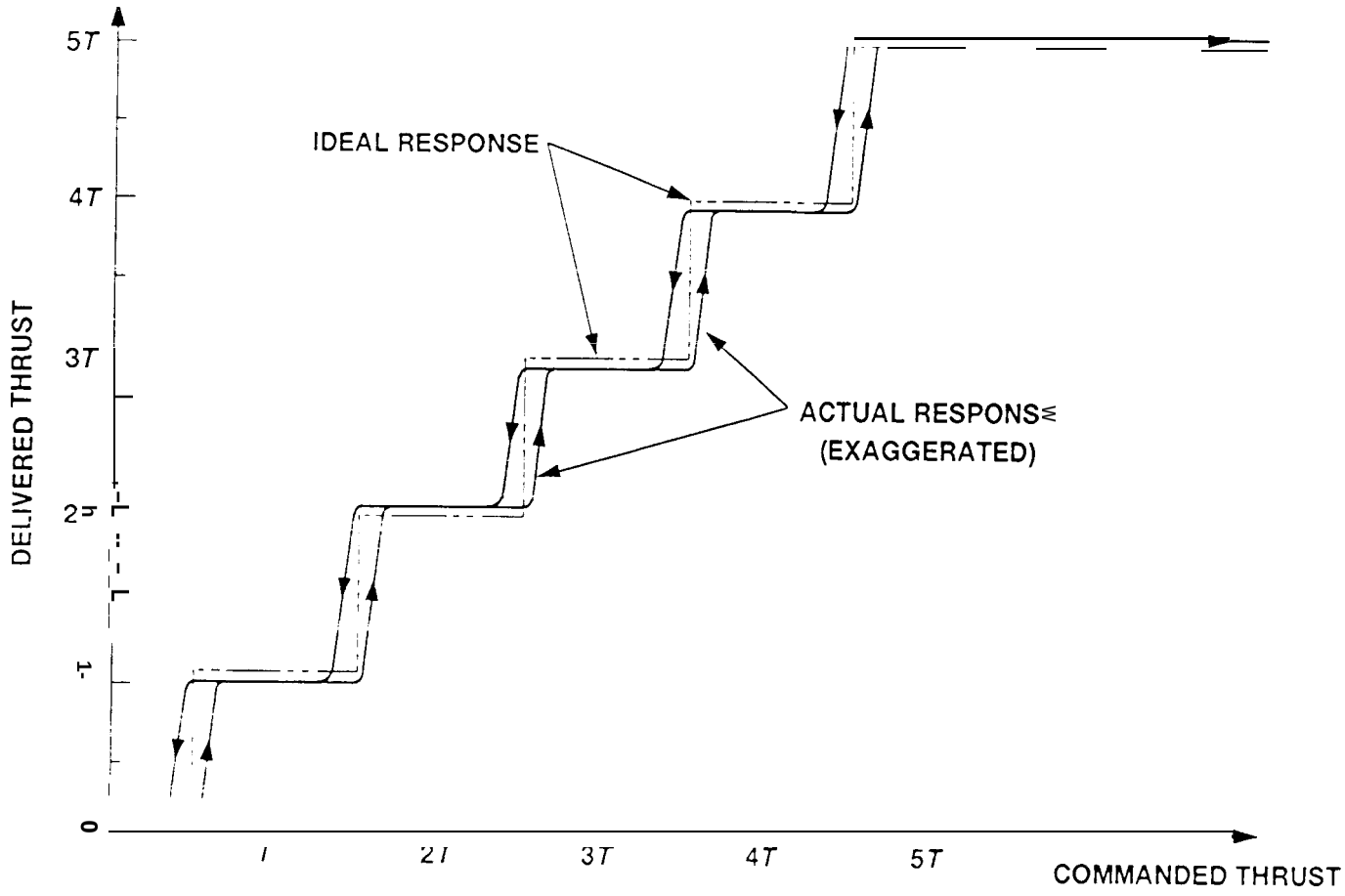

Figure 3: Switching Curve for Clustered Engine Configuration

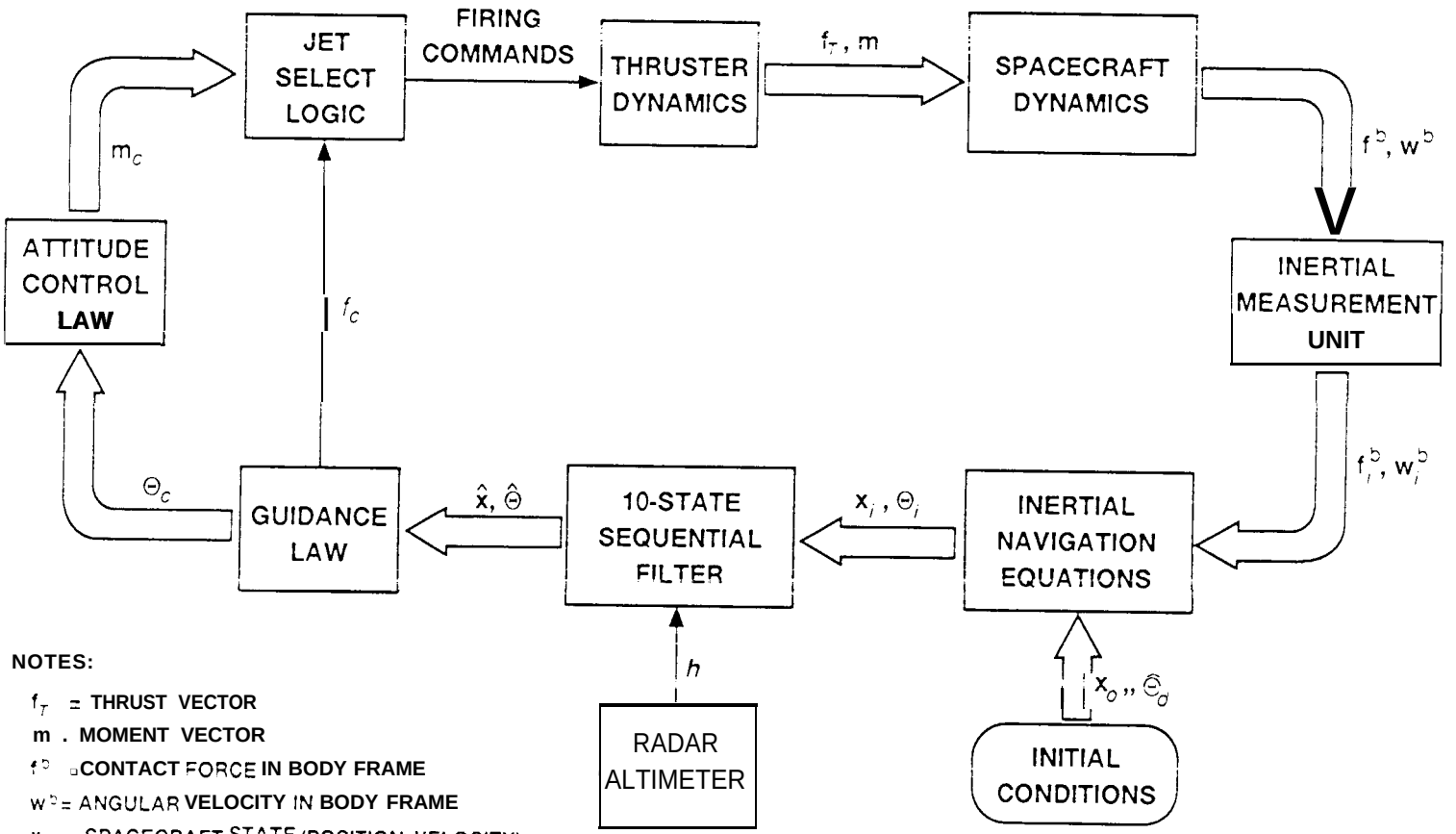

Figure 4: Mars Lander Guidance, Navigation and Control System

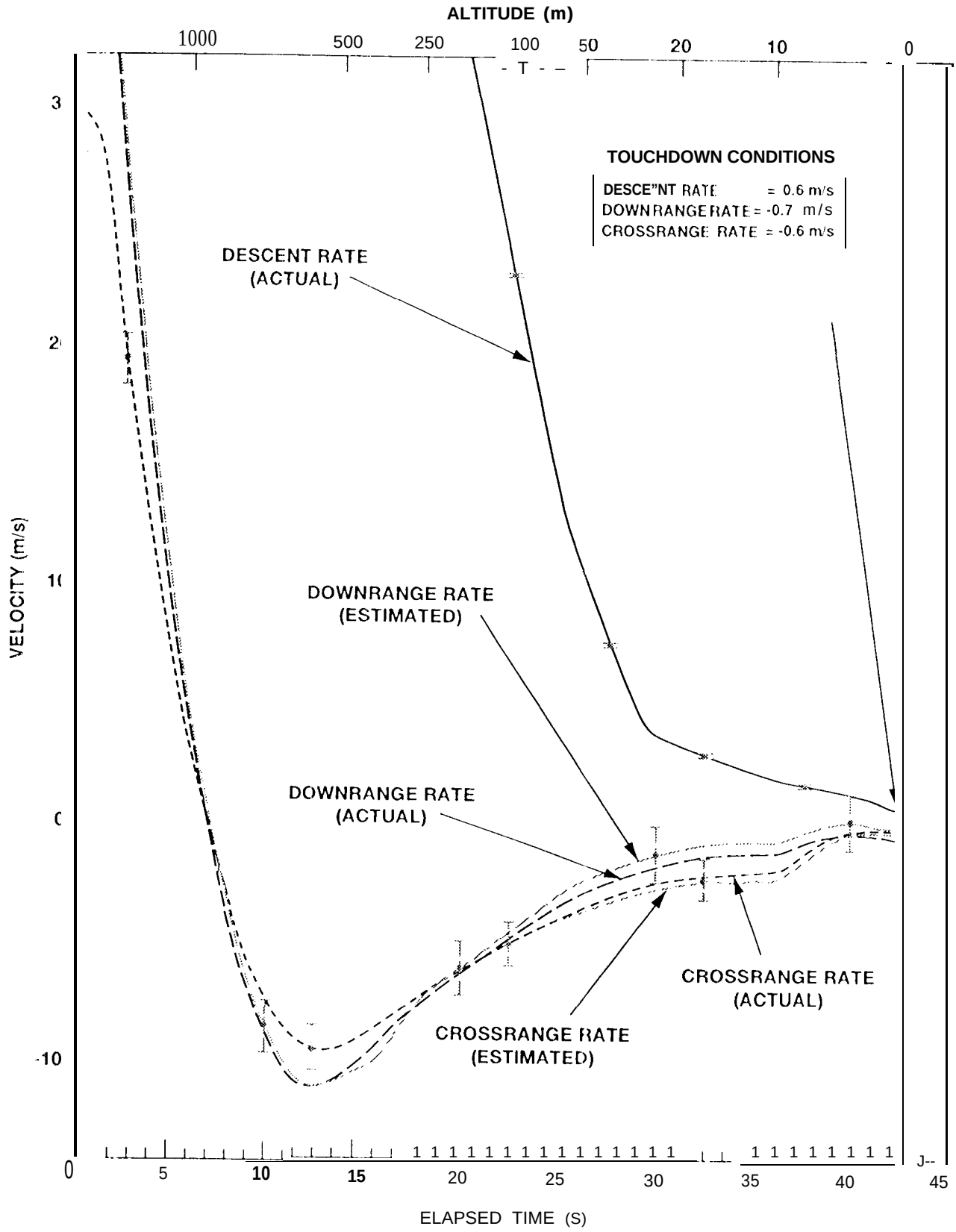

NOTE: ERROR BARS Represent" ±1σ DEVIATIONS

Figure 6: Velocity Vector Components (Simulation Case 3)

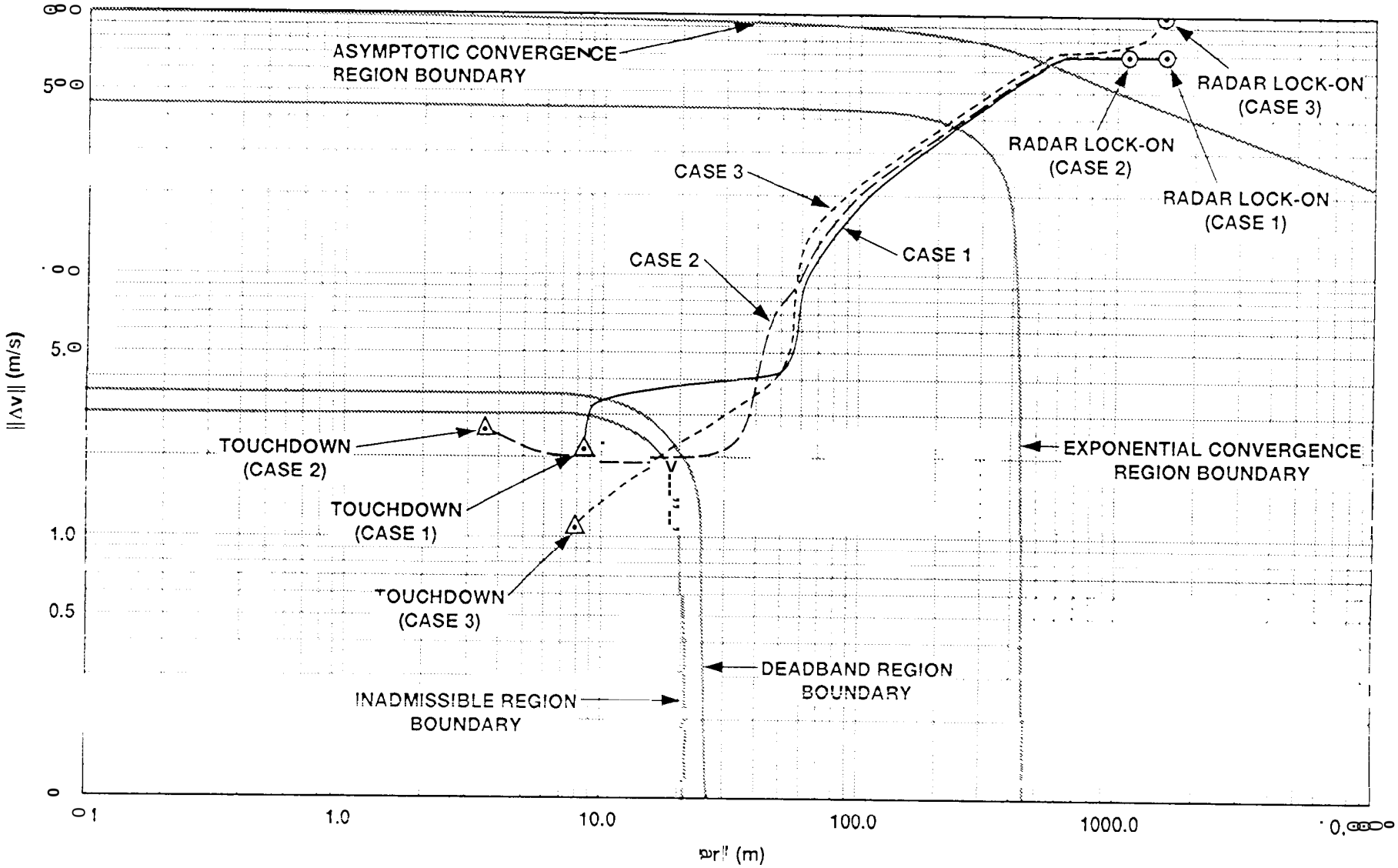

Figure 5: Position-Velocity Magnitude Map of Simulation Cases

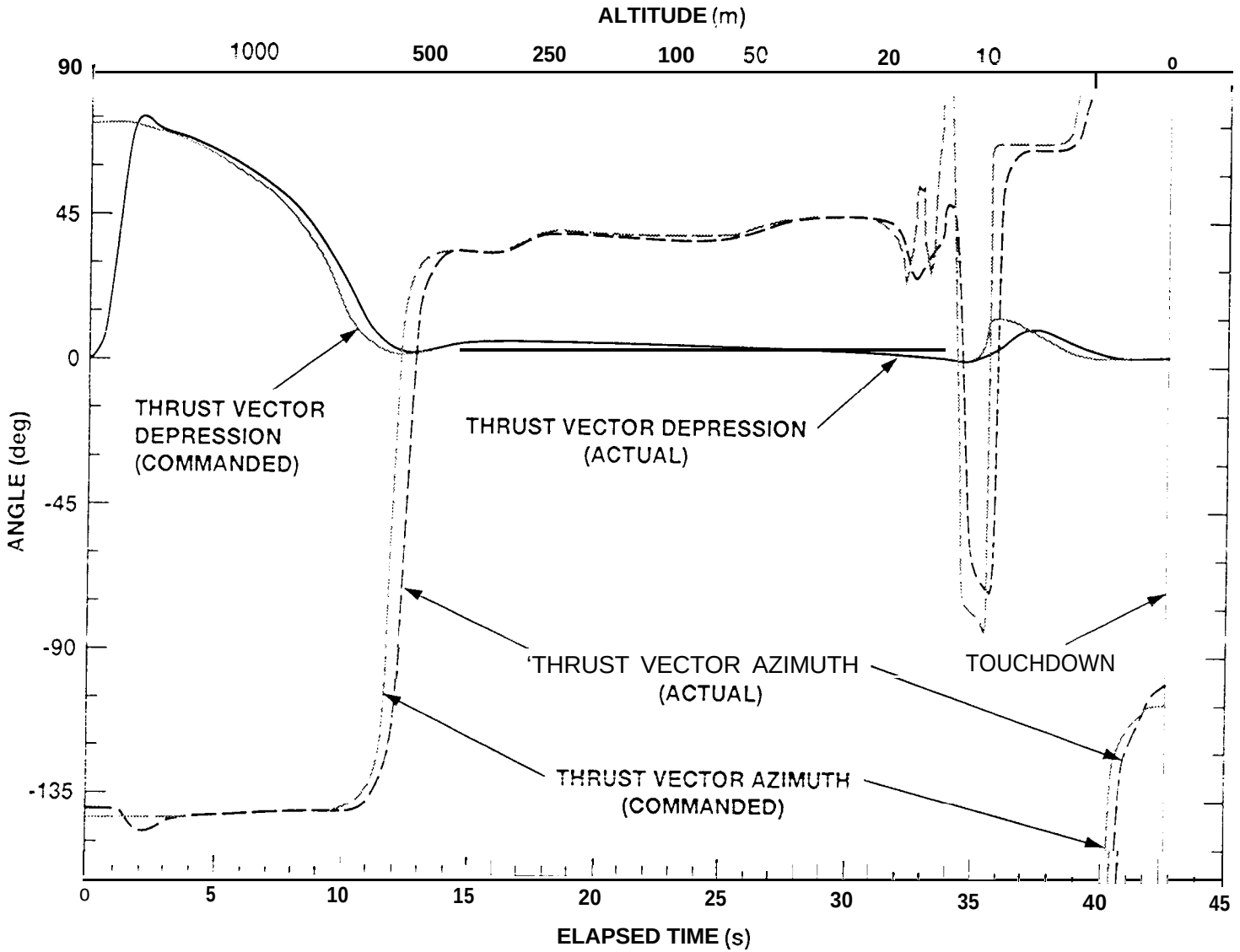

Figure 7: Thrust Vector Orientation (Simulation Case 3)

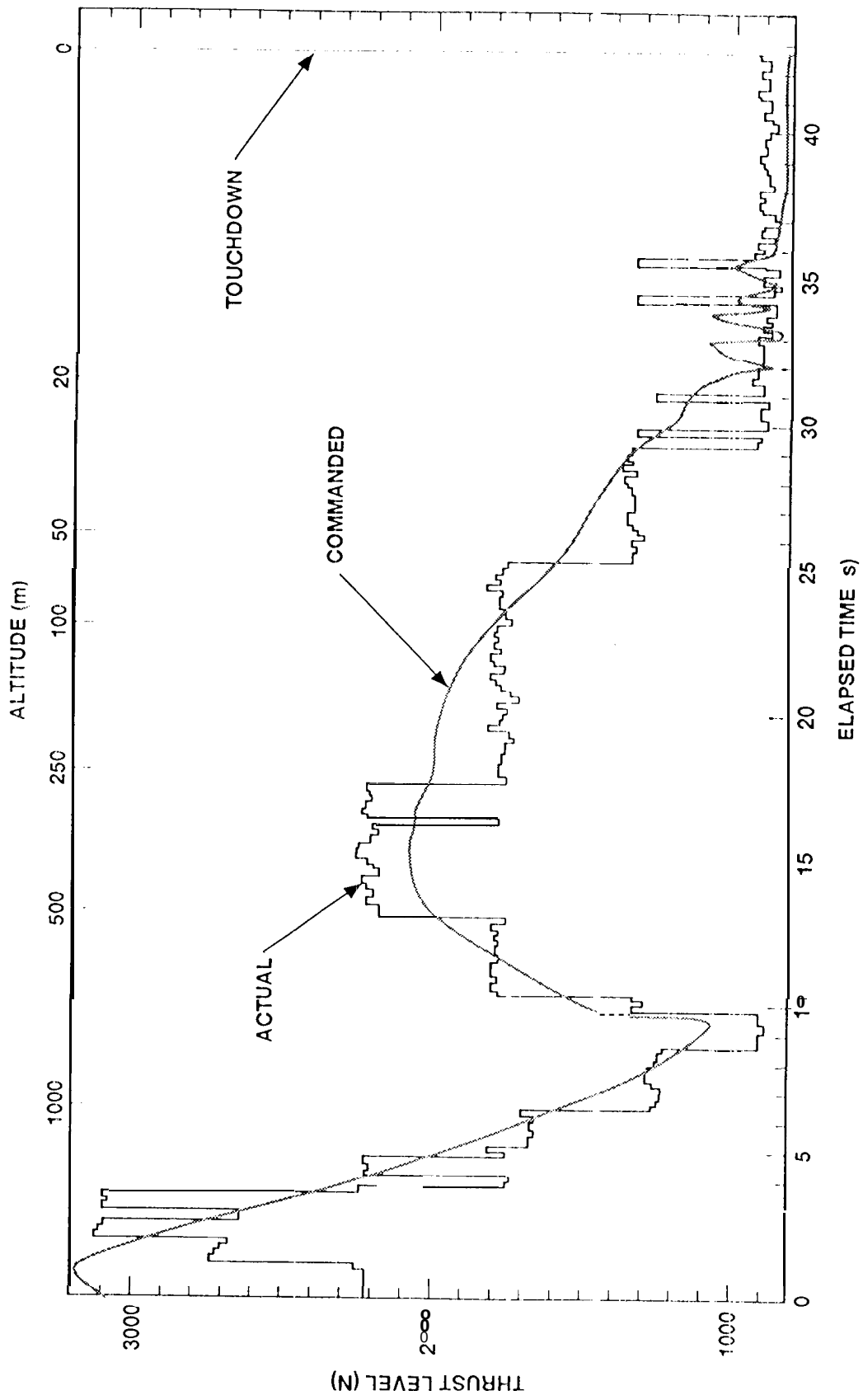

Figure 8: Thrust Magnitude (Simulation Case 3)